Desalination and Water Treatment
www.deswater.com

doi: 10.5004/dwt.2020.25879

201 (2020) 250–260
October

Enhanced adsorption of As(V) from aqueous solution by mesoporous goethite: kinetics, isotherms, thermodynamics, and mechanism

Yujie Zhao[a], Min Xiao[b,*], Shan Zhao[b], Hongtao Fan[c,*]

[a]*Key Laboratory for Environmental Factors Control of Agro-Product Quality Safety, MOA, Tianjin 300191, China, email: yujiezhao@126.com (Y.J. Zhao)*
[b]*College of Environment, Shenyang University, Shenyang 110044, China, emails: xyz012263@163.com (M. Xiao), 1805825202@qq.com (S. Zhao)*
[c]*College of Chemical Engineering and Environmental Engineering, Liaoning Shihua University, Fushun 113001, China, email: httyf_77@163.com (H.T. Fan)*

Received 27 July 2019; Accepted 23 March 2020

ABSTRACT

As(V) adsorption capacity on mesoporous goethite was investigated and compared to common goethite. The mesoporous goethite synthesized by a hydrothermal method possessed the larger pore size and mesopore volume than common goethite. The kinetics, isotherms, thermodynamics, and As(V) adsorption mechanism on the mesoporous goethite were thoroughly studied. The kinetics data of As(V) adsorption on mesoporous goethite fitted well the pseudo-second-order equation, and the isotherm data fitted better with the Langmuir model. The maximum As(V) adsorption capacity of mesoporous goethite derived from the Langmuir model is 41.19 mg/g at 25°C, which is much higher than those of natural or modified goethite. The thermodynamic parameter ($\Delta G°$ and $\Delta H°$) showed that the As(V) adsorption process was spontaneous and exothermic. The Fourier-transform infrared spectroscopy, Raman and X-ray photoelectron spectroscopy results revealed that the As(V) removal mechanism can be due to the surface complexation of As(V) and mesoporous goethite. These results show that the mesoporous goethite is a promising efficient and easy to prepare adsorbent for removal of As(V) from water.

Keywords: Goethite; Arsenic; Mesoporous; Adsorption

1. Introduction

Arsenic (As), known to be highly toxic and carcinogenic, has attracted increasing attention as a result of the wide release of arsenic-contaminated wastewater into the natural environment from mining or smelting activity [1–4]. Arsenic often has four oxidation states (–III, 0, III, V), and the most occurring forms are III and V in natural environments, depending on the pH and redox potential [1]. Although the toxicity of As(III) is much higher than As(V), As(V) is much more mobile and soluble and is the primary form in oxic conditions [1]. It is well known that many techniques such as ion-exchange, co-precipitation, flocculation, membrane technology, and adsorption have been used to remove As from wastewater [5–15]. Compared to traditional precipitation methods, adsorption has the advantage of high efficiency and low-cost [16–25]. A great many new adsorption materials (e.g., graphene composites and metal organic frameworks) had been reported to remove arsenic effectively from aqueous solution. However, the

* Corresponding authors.

preparation processes of these new materials are complex, expensive, and not appropriate for industrial applications on a large scale [26–29]. Iron oxides or oxyhydroxides have been comprehensively used in the adsorption process of pollution because they have a strong affinity with anion species [30–36]. More importantly, they are widely distributed in nature and can be synthesized readily on a large scale [31]. For example, Zhao et al. [32] reported the adsorption and heterogeneous catalytic oxidation of As(III) on ferrihydrite. Guo et al. [33] investigated the adsorption behaviors and surface structure of antimony (III/V) on iron oxides. The results indicated that the affinity of Sb(V) and Sb(III) toward the iron oxides was related to the Sb species, solution pH, and the nature of iron oxides. As we know, goethite is the most stable iron oxyhydroxide in the natural environment and has excellent surface activity. So, natural goethite or synthetic goethite have been widely used for removing heavy metals from wastewater (such as As(V), Sb(V), Cr(V)). However, in the previous studies, the adsorption capacity of As(V) on natural or synthesized goethite is still limited [30–36]. Recently, the preparation of 3D hierarchical hollow goethite or mesoporous goethite has been supposed to be an effective method to enhance pollutant adsorption properties [37,38]. However, the organic solvent (such as glycerol, ethylene glycol) often was involved in the synthesis process. The objective of this work to prepare mesoporous goethite with a high specific surface area by a simple solvent-free hydrothermal method and investigate its adsorption capacity of As(V) from aqueous solution.

In the present work, the physicochemical characteristics of mesoporous goethite, adsorption kinetics, isotherms, thermodynamic analysis, and mechanism were studied. The research results are expected to provide some useful information for industrial wastewater treatment on a large scale in the future.

2. Experimental setup

2.1. Materials

Ferrous sulfate heptahydrate, ferric nitrate nonahydrate, hydrogen peroxide (30%), potassium pyroantimonate, sodium hydroxide, hydrochloric acid, and sodium borohydride were obtained from Adamas Reagent, Ltd. Arsenate stock solutions (500 mg/L) were prepared by dissolving $Na_2HAsO_4{\cdot}7H_2O$ into ultrapure water.

2.2. Synthesis of mesoporous goethite

The mesoporous goethite was synthesized by the oxidation of ferrous sulfate heptahydrate with hydrogen peroxide in aqueous solution following the method reported by Dong et al. [39] and Xiao et al. [40]. Typically, 0.70 g ferrous sulfate heptahydrate was added to 21.0 g ultrapure water, and then 30% hydrogen peroxide (6.0 mL) was added to the solution mentioned above under vigorous stirring to obtain a homogeneous yellow slurry solution. Then the suspension was transferred into a polytetrafluoroethylene lined hydrothermal synthesis reactor maintaining 150°C for 6 h. At last, the solid product was centrifuged and rinsed with ultrapure water for several times until the supernatant was near neutral and dried under vacuum at 80°C overnight. Meanwhile, common goethite was prepared as contrast by the method of Schwertmann and Cornell [41].

2.3. Characterization

The crystal structure of mesoporous goethite was characterized by X-ray diffraction (XRD) (Bruker D8 Advance, Germany). The field emission scanning electron microscopy (FE-SEM; ZEISS Gemini 300, Germany) and transmission electron microscopy (TEM; Tecnai G220, USA) were used to observe the surface morphology of mesoporous goethite. Based on nitrogen adsorption–desorption isotherm, the Brunauer–Emmett–Teller (BET) surface areas, the Barrett–Joyner–Halenda (BJH) average pore diameters, mesoporous volumes, and the total pore volumes were calculated (Quantachrome Autosorb 1-C, USA). Fourier-transform infrared (FT-IR) spectra of mesoporous goethite were recorded in the range 400–1,000 cm^{-1} using the KBr pellet technique (Thermo Nicolet NEXUS 470, USA). Raman spectra were recorded at ambient temperature with a confocal laser micro Raman Spectrometer with a laser power of 2 mW (ThermoFisher DXR780, USA). The chemical species of the surface O and As elements on mesoporous goethite before and after As(V) adsorption were determined by an X-ray photoelectron spectrometer (Thermo Scientific 250Xi, USA). Zeta potential analysis was conducted on a Malvern Zetasizer Nano (Malvern, UK). The hydride generation-atomic fluorescence spectrometry was used to detect the As(V) concentration (Jinsuokun SK-2003AZ, China) [5].

2.4. Adsorption study

Adsorption experiments were carried out using 10 mg/L As(V) solutions. During the kinetic experiments, the As(V) solution was taken out from the suspensions at the different intervals (5–60 min), and then the As(V) concentration was detected momentarily. The adsorption isotherms of As(V) on the mesoporous goethite at different temperatures (25°C, 35°C, and 45°C) were investigated. The suspensions were shaken continuously until the adsorption equilibrium was reached. In both cases, the suspensions were also centrifuged and then filtered immediately through a 0.45 μm microfiltration membrane.

The concentration of As(V) in the filtrate was then analyzed by a hydride generation-atomic fluorescence spectrophotometer. The adsorption capacity of As(V) can be got from the experiment data according to the following equation [42,43]:

$$Q_t = \frac{\left(C_0 - C_t\right)}{1{,}000m} \tag{1}$$

where Q_t represents the adsorption capacity of As(V) at t min (mg/g); C_t and C_f are the As(V) concentrations of initial and t min (mg/L), respectively. V is the As(V) solution volume. m is the weight of sorbent (g).

Meanwhile, the effect of goethite dosage, initial As(V) solution pH value, co-existing ions on the As(V) adsorption capacity were investigated in batch experiments, respectively.

2.5. Re-usability of mesoporous goethite

Desorption/re-usability tests of As(V) on the mesoporous goethite were performed by treatment of the As(V)-loaded mesoporous goethite with 1 M NaOH solution for 4 h. Then, the sorbent was taken out, washed, and reused again. Desorption/re-usability tests were repeated eight times to evaluate the re-usability of mesoporous goethite.

3. Results and discussion

3.1. Characterization

The crystal structure and surface morphology of mesoporous goethite were characterized and shown in Fig. 1. As shown in Fig. 1a, the diffraction pattern for mesoporous goethite exhibits typical characteristic peaks at 21.22°, 33.24°, 34.70°, 36.65°, 41.68°, 53.24°, 59.02°, 61.38°, and 63.97°, corresponding to (110), (130), (021), (111), (140), (221), (151), (002), and (061) of goethite (JCPDS no. 29–0713), respectively [39]. The diffraction peaks of goethite were sharp and intense, indicating their highly crystalline nature. No impurity peaks were observed, confirming the high purity of the prepared goethite. The FE-SEM image of mesoporous goethite (Fig. 1b) presented the spindly dispersed particles essentially with a maximum diameter of about 30 nm and a length of about 100 nm.

The morphology of mesoporous goethite was also characterized using TEM, and the image is shown in Fig. 2. The image of mesoporous goethite presented many spindly substances with decades of a nanometer in width and hundreds of nanometers in length. The corresponding energy-dispersive X-ray spectroscopy analysis suggested that the goethite contained iron and oxygen.

Fig. 3 presents the FT-IR (a) and Raman (b) spectra of mesoporous goethite. The intense band at 3,140 cm^{-1} was assigned to the bulk hydroxyl stretch of goethite. The absorption bands at 882 and 786 cm^{-1} were attributed to the Fe–O–H bending vibrations of goethite. The band near 1,648 cm^{-1} due to the bending deformation of water molecules was observed at 3,140 cm^{-1}. As shown in Fig. 3b, two sharp peaks observed at 296 and 387 cm^{-1}, and the band positions in range 242, 477, and 546 cm^{-1} were in good agreement with the characteristic bands of goethite structure [41].

Nitrogen gas adsorption-desorption isotherms and BJH desorption pore size distributions of common goethite (a) and mesoporous goethite (b) were shown in Fig. 4. The specific surface area and pore parameters of the common goethite and mesoporous goethite obtained by the nitrogen adsorption and desorption isotherms were listed in Table 1. The adsorption–desorption isotherm curves of mesoporous goethite (b) exhibit a type IV isotherm with H3 hysteresis loop, indicating the presence of mesoporous in goethite. However, the adsorption–desorption isotherm curves of common goethite (a) exhibit a type III isotherm, and the hysteresis loop becomes inconspicuous, indicating no typical pores appearance. As listed in Table 1, the BET specific surface area of mesoporous goethite and common goethite is calculated to be 186.25 and 142.23 m^2/g, respectively. The pore parameter properties of the mesoporous goethite are so much better than those of common goethite, for example, the total pore volume, micropore volume, BJH desorption average pore diameter, especially mesopore volume. The larger pore size and mesopore volume of mesoporous goethite probably possessed more active site, and then lead to the higher adsorption capacity of As(V) under the same conditions In addition, the zeta potential profile of the mesoporous goethite vs. pH in aqueous solution was determined and shown in Fig. S1.

3.2. Effect of dosage

Fig. 5 presents the effect of adsorbent dosage on the As(V) removal rate on mesoporous goethite. As we can see, the removal rate rises with increasing mesoporous

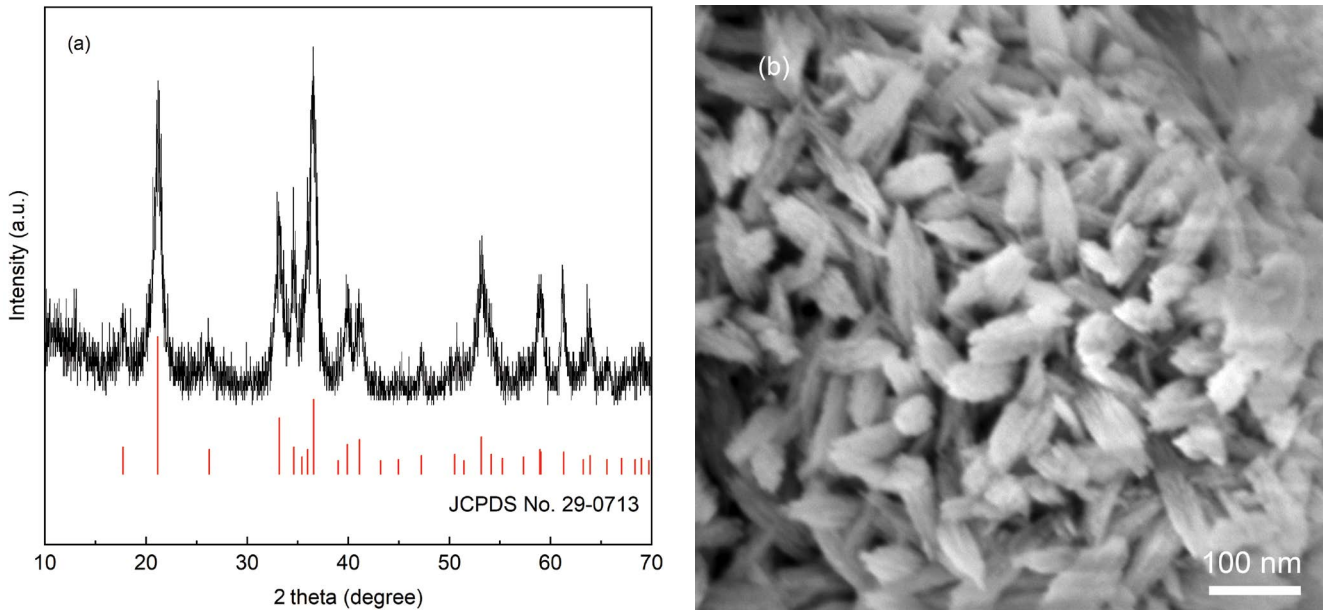

Fig. 1. (a) XRD pattern and (b) FE-SEM image of mesoporous goethite.

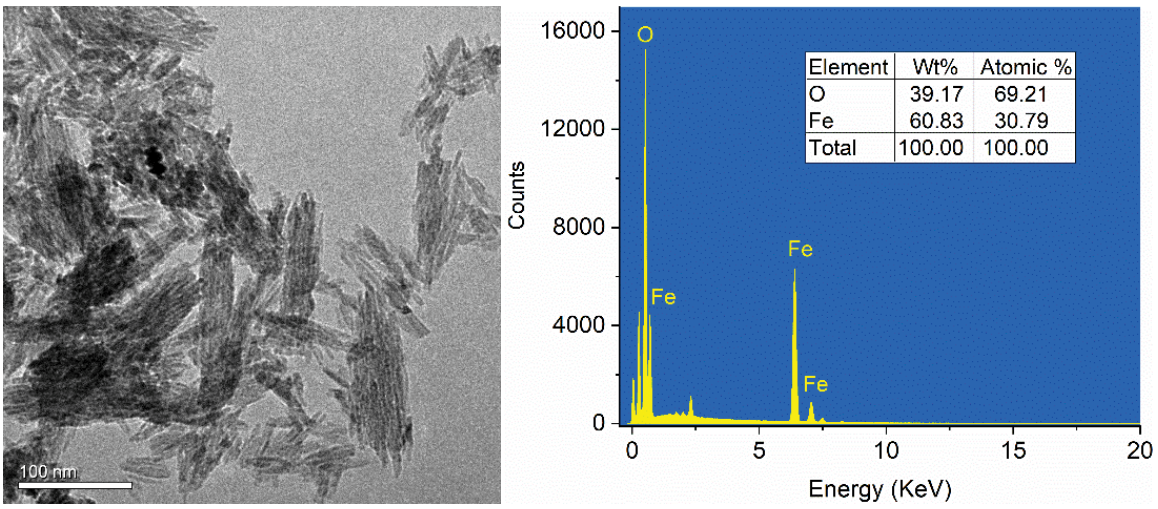

Fig. 2. TEM image and corresponding energy-dispersive X-ray spectroscopy of mesoporous goethite.

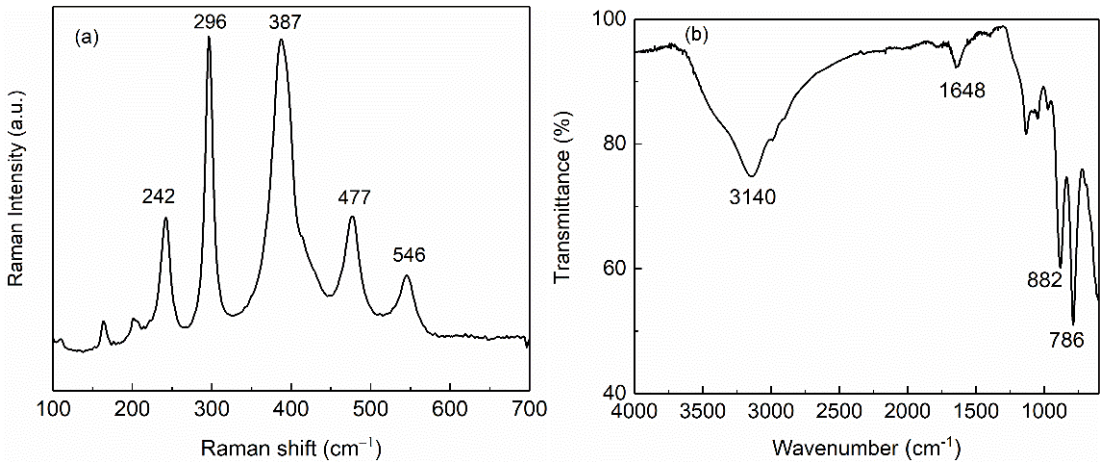

Fig. 3. Raman and FT-IR spectra of mesoporous goethite.

goethite dosage until it reaches 100% when the adsorbent dosage is 1 g/L. For comparing the adsorption capacity of As(V) between mesoporous goethite and common goethite, the adsorbent dosage was set to be 0.5 g/L in the following work.

3.3. Effect of initial As(V) solution pH

Fig. 6 shows As(V) adsorption on mesoporous goethite is strongly dependent on the initial solution pH. The adsorption capacity of As(V) was gradually decreased with the solution pH increasing from 4.0 to 9.0. It's well known that in water solution, the $H_2AsO_4^-$ is the primary specie of As(V) at pH 3.0–6.0, while the dominant species of As(V) are $HAsO_4^{2-}$ and AsO_4^{3-} when solution pH is higher than 6.0. As a result, $H_2AsO_4^-$ can be adsorbed readily on the positively charged surface of goethite under low pH conditions. On the other hand, as the solution pH increases, the negative charge goethite surface brings about strong electrostatic repulsion with As(V) species ($HAsO_4^{2-}$ and AsO_4^{3-}), which causes adsorption capacity of As(V) decrease [4].

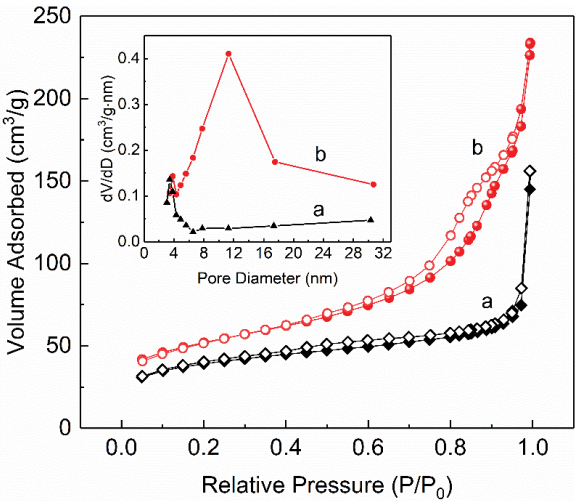

Fig. 4. Nitrogen gas adsorption–desorption isotherms and BJH desorption pore size distributions (inset) of (a) common goethite and (b) mesoporous goethite.

Table 1
Specific surface area and pore parameters of the common goethite and mesoporous goethite

Sample	S_{BET}[a] (m^2/g)	V_{tot}[b] (cm^3/g)	V_{mic}[c] (cm^3/g)	V_{mes}[d] (cm^3/g)	D_{BJH}[e] (nm)
Common goethite	142.33	0.242	0.058	0.054	6.786
Mesoporous goethite	186.25	0.362	0.076	0.223	7.768

[a]BET surface area;
[b]Total pore volume;
[c]Micropore volume;
[d]Mesopore volume;
[e]BJH desorption average pore diameter.

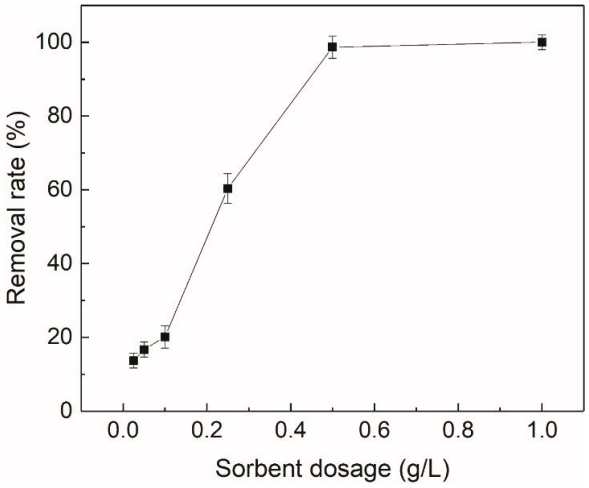

Fig. 5. Effect of mesoporous goethite dosage on As(V) removal rate (C_0: 10 mg/L; initial pH: 7.0; T: 25°C; adsorption time: 2 h).

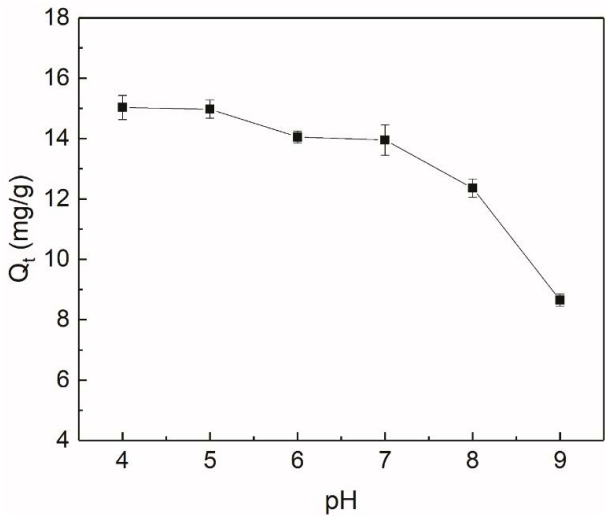

Fig. 6. Effect of pH on As(V) adsorption on mesoporous goethite (C_0: 10 mg/L; adsorbent dosage: 0.5 mg/g; T: 25°C; adsorption time: 2 h).

3.4. Adsorption kinetics

Fig. 7 shows the As(V) adsorption kinetics curves on common goethite and mesoporous goethite. Adsorption equilibrium was reached within about 60 min for mesoporous goethite, but for common goethite, it would take about 150 min. The adsorption kinetics data were fitted with pseudo-first-model and pseudo-second-model [43–45], respectively. The results of the kinetics parameters were listed in Table 2. As we can see, the pseudo-second-order equation can describe well the adsorption data with a correlation coefficient (R^2 > 0.998). In Table. 2, it could be found that the As(V) adoption rate constant (k_2) on mesoporous goethite is twice as large as that on common goethite, which could result from the more adsorption site and higher mesoporous volume of mesoporous goethite.

3.5. Effect of co-ions

The effect of co-ions on the As(V) sorption was studied in the presence of citrate and phosphate with a concentration of 10 mg/L. The results plotted in Fig. 8 show that As(V) adsorption on mesoporous goethite could be influenced by citrate and phosphate, especially with phosphate, the As(V) adsorption capacity reduced markedly from 16.54 to 11.23 mg/L. As we know, phosphate is a typical competitive oxyanion to As(V) because its molecular structure is analogous to that of As(V) [46].

3.6. Adsorption isotherms

Fig. 9 shows the adsorption isotherms of As(V) on the mesoporous goethite at different temperatures (25°C, 30°C, and 35°C). The Langmuir, the Freundlich, and the Temkin models [47–49] were used to analyze the isotherm data (Fig. S2a–c) and calculated the model's parameters are listed in Table 3. It was found that the Langmuir model was fitted well with experimental data. The correlation coefficients (R^2) of the Langmuir model were between 0.9883 and 0.9944 at 25°C–35°C. Meanwhile, the experimental data were further fitted by Freundlich and Temkin model. The correlation coefficients of the Freundlich model (R^2 = 0.9015–0.9487) and the Temkin model (R^2 = 0.9509–0.9629) were less than those of the Langmuir model. The higher correlation of the Langmuir model indicated that the adsorption process of As(V) ions onto mesoporous goethite was monolayer adsorption.

Meanwhile, the effect of temperature on isotherm was examined at different temperatures, and the As(V) adsorption thermodynamic parameters can be obtained (Fig. S2d). The Gibbs free energy ($\Delta G°$, kJ/mol), enthalpy ($\Delta H°$, kJ/mol) and entropy ($\Delta S°$, J/mol K) for As(V) adsorption can be calculated by Eqs. (2) and (3) [43], and the results of thermodynamic parameters are listed in Table 4. From

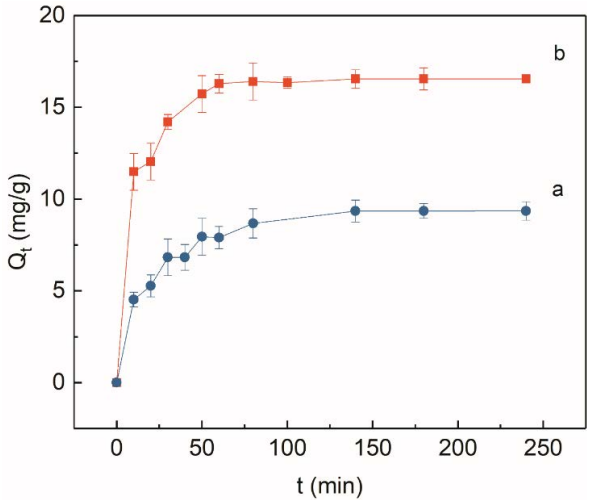

Fig. 7. Adsorption kinetics of As(V) on (a) common goethite and (b) mesoporous goethite (C_0: 10 mg/L; T: 25°C; adsorbent dosage: 0.5 g/L; initial pH: 7.0).

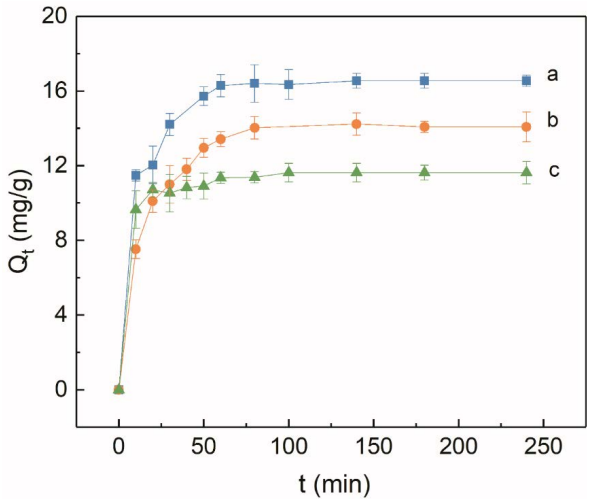

Fig. 8. Effect of co-ions on As(V) adsorption: (a) blank, (b) citrate, and (c) phosphate (C_0: 10 mg/L; co-ions concentration: 10 mg/L; T: 25°C; adsorbent dosage: 0.5 g/L; initial pH: 7.0).

Table 2
Adsorption kinetics parameters for As(V) on mesoporous goethite and conventional goethite

Model	Parameters	Common goethite	Mesoporous goethite
Pseudo-first-order	k_1 (min^{-1})	0.064	0.3548
	Q_e (mg/g)	76.96	56.51
	R^2	0.7750	0.9579
	RSS[a]	1.494	0.098
Pseudo-second-order	k_2 (mg/g min)	0.006	0.012
	Q_e (mg/g)	10.05	16.98
	R^2	0.9994	0.9984
	RSS	0.0921	0.7388
Intraparticle diffusion	k_{p1} (mg/g min$^{0.5}$)	1.125	0.865
	R^2	0.9524	0.9320
	RSS	0.6558	0.3812
	k_{p2} (mg/g min$^{0.5}$)	0.029	0.177
	R^2	0.5294	0.6845
	RSS	0.0129	0.3917

[a]Residual sum of squares

Table 4, the $\Delta G°$ and $\Delta H°$ are negative, indicating the adsorption process is spontaneous and exothermic.

$$\Delta G° = -RT\ln K \quad (2)$$

$$\ln K = \frac{\Delta S°}{R} - \frac{\Delta H°}{RT} \quad (3)$$

3.7. Adsorption mechanism

The mesoporous goethite before and after As(V) adsorption was characterized by FT-IR, Raman, and X-ray photoelectron spectroscopy (XPS) analysis to clarify the potential adsorption mechanism. FT-IR and Raman spectra of mesoporous goethite before and after adsorption As(V) were shown in Fig. 10. As sown in Fig. 10a, the absorption bands at ca. 892 and 795 cm^{-1} can be ascribed to the in and out the plane of Fe–OH in mesoporous goethite. Furthermore, Fe–O symmetrical stretching vibration band can be found at ca. 630 cm^{-1}. Because the IR absorption bands of As–O or As–OH are located near 808 and 878 cm^{-1} [50], it is difficult to determine the existence of As(V) on mesoporous goethite after adsorption. However, after adsorption of As(V), the relative intensities of the bands at ca. 892 and 795 cm^{-1} to that of ca. 630 cm^{-1} increases obviously, which could be caused by the replacement of hydroxyl groups existed on mesoporous goethite with arsenate by surface complexation. The Raman spectra of mesoporous goethite before and after adsorption As(V) were also be detected and shown in Fig. 10b. A weak shoulder peak at ca. 858 cm^{-1} can be

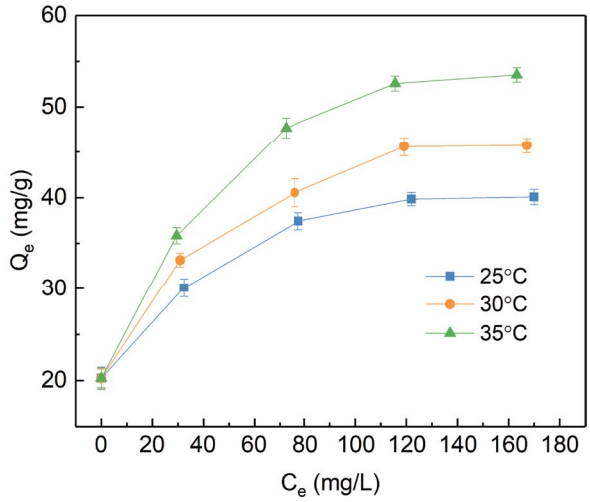

Fig. 9. As(V) adsorption isotherms on mesoporous goethite.

found after As(V) adsorption, which in the future confirmed the assumption on the result of IR characterization [51].

To further investigate the interaction of As(V) and mesoporous goethite and the adsorption mechanism, the mesoporous goethite before and after adsorption As(V) was further characterized by XPS analysis (Fig. 11). For the mesoporous goethite after As(V) adsorption, the peaks locating at 45.23 eV can be assigned to As 3d. The O 1s spectra of mesoporous goethite, shown in Fig. 11b can be deconvoluted into three peaks at about 530.0, 531.3, and 532.2 eV, respectively. The peak at 530.0 eV can be attributed to the lattice oxygen binding with Fe (denoted as M–O). The peak at 531.3 eV can be assigned to the lattice hydroxyl groups (denoted as M–OH). The peak at 532.2 eV can be assigned to the adsorbed water (denoted as H_2O) [52]. After adsorption, the content of M–OH decreased from 55.5% to 52.7%, and the apparent increase from 27.7% to 36.3% was found for M–O content, which shows that some hydroxyl groups on mesoporous goethite were partly bonded with As(V) by surface complexation. Therefore, the XPS analysis demonstrates the As(V) adsorption mechanism on mesoporous goethite was the replacement of hydroxyl groups existed on mesoporous goethite with arsenate by surface complexation. However, to determine the kinds of

Table 3
Adsorption isotherm parameters for As(V) on mesoporous goethite at different temperatures

Model	Parameters	Temperature (°C)		
		25	35	45
Langmuir	Q_{max} (mg/g)	41.19	47.24	55.56
	b (L/mg)	0.175	0.141	0.122
	R^2	0.9944	0.9907	0.9883
	RSS (×10³)	0.0504	0.0649	0.1704
Freundlich	k_f (mg/g)(L/mg)$^{1/n}$	16.43	16.74	16.08
	n	5.541	4.942	4.096
	R^2	0.9015	0.9487	0.9320
	RSS (×10³)	13.49	18.07	22.16
Temkin	A (L/mg)	–49.947	–43.717	–41.046
	B (kJ/mol)	52.410	53.623	55.983
	R^2	0.9509	0.9584	0.9629
	RSS (×10³)	0.8444	0.7471	0.7600

Table 4
Thermodynamic parameters of As(V) adsorption on mesoporous goethite

T/K	$\Delta G°$ (kJ/mol)	$\Delta H°$ (kJ/mol)	$\Delta S°$ (J/mol K)
298.15	–23.51		
303.15	–23.75	–27.99	–15.10
308.15	–24.12		

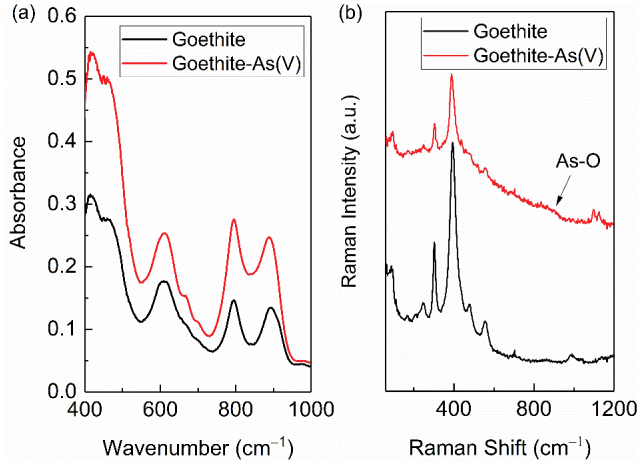

Fig. 10. (a) FT-IR and (b) Raman spectra of mesoporous goethite before and after adsorption As(V).

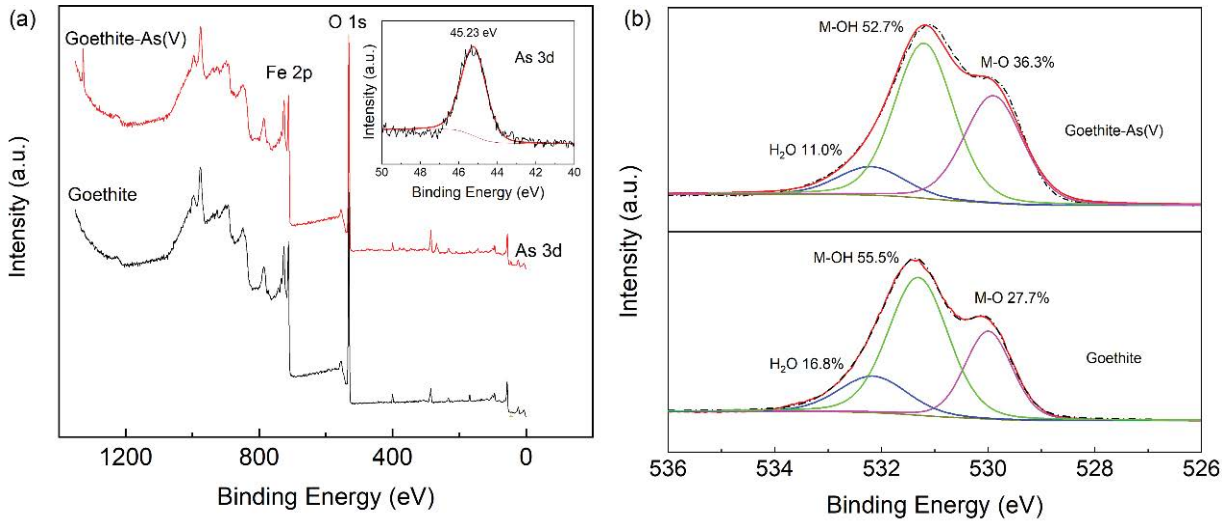

Fig. 11. (a) XPS survey spectra and (b) peaks for O 1s of mesoporous goethite before and after adsorption As(V).

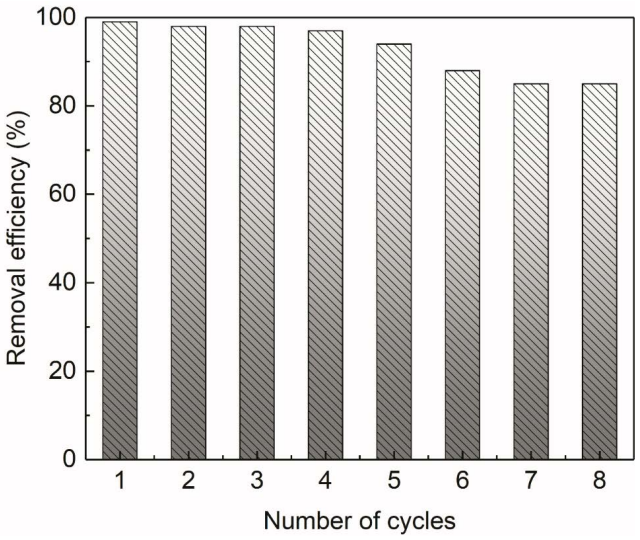

Fig. 12. Re-usability of mesoporous goethite for As(V) (C_0: 10 mg/L; initial pH: 7.0; T: 25°C).

complexes formed on goethite extended X-ray absorption fine structure (EXAFS) spectroscopy are needed to apply.

From Table 3, the adsorption capacity of As(V) on the mesoporous goethite is 41.19 mg/g at 25°C. Compared with previous reported goethite-related adsorbent, the As(V) adsorption capacity of the mesoporous goethite is higher than those of natural or modified goethite listed in Table 5. Because the mesoporous goethite exhibits the higher specific surface area, porosity (Table 1), and the monolayer adsorption (Table 3), the better As(V) adsorption capacity can be got.

3.8. Re-usability of mesoporous goethite

The re-usability for sorbent is one of the notable performances in the process of the actual application. The consecutive As(V) sorption-regeneration cycles on the mesoporous goethite have been repeated eight times, and the results are shown in Fig. 12. The removal efficiency of As(V) on mesoporous goethite is more than 90% for four cycles, and higher than 84% for eight cycles. The result shows the mesoporous goethite exhibits excellent reuse ability.

4. Conclusion

Mesoporous goethite was synthesized by the hydrothermal method without organic solvent. The XRD and FE-SEM characterization revealed that prepared goethite exhibits high crystallinity and spindly dispersed particles with a maximum diameter of about 30 nm and a length of about 100 nm. The mesoporous goethite showed excellent As(V) removal capacity in comparison with the natural and modified goethite reported in the literature. The batch experiment results show As(V) adsorption kinetics data on mesoporous goethite was fitted well to the pseudo-second-order equation, and the maximum adsorption of As(V) on mesoporous goethite calculated by the Langmuir isotherm model was 41.19 mg/g. Surface complexation via replacement of hydroxyl groups existed on mesoporous goethite with arsenate may be the dominant adsorption mechanism.

Table 5
Comparison of the maximum adsorption capacity of As(V) among mesoporous goethite and other related adsorbents

Adsorbents	pH	Adsorption capacities (mg/g)	References
FeOOH/chitosan	6.0[a]	5.49	[53]
FeOOH	6.0[a]	28.57	[35]
Fe_3O_4/goethite	Unadjusted	30.20	[54]
Goethite/polyethylene glycol/multi-walled carbon nanotube	6.0[a]	49.39	[55]
Goethite nanorods	Unadjusted	30.64	[56]
Goethite	4.0[b]	5.03	[57]
Goethite	2.3[b]	13.47	[57]
Natural goethite (55%)	4.0[a]	6.20	[58]
Natural goethite (87%)	5.5[a]	12.40	[59]
Natural goethite	7.5[b]	0.45	[57]
Mesoporous goethite	7.0[a]	41.19	This work

[a]Initial pH;
[b]Equilibrium pH.

Acknowledgment

We thank the opening fund of Key Laboratory for environmental factors control of Agro-product quality safety (18nynzahj-2), the National Natural Science Foundation of China (No. 21607107) for the financial support.

References

[1] J.Y. Wang, T.P. Zhang, M. Li, Y. Yang, P. Lu, P. Ning, Q. Wang, Arsenic removal from water/wastewater using layered double hydroxide derived adsorbents, a critical review, RSC Adv., 8 (2018) 22694–22709.
[2] B.A. Marinho, R.O. Cristóvão, R.A.R. Boaventura, V.J.P. Vilar, As(III) and Cr(VI) oxyanion removal from water by advanced oxidation/reduction processes–a review, Environ. Sci. Pollut. Res., 26 (2019) 2203–2227.
[3] F. Ogata, E. Ueta, N. Kawasaki, Characteristics of a novel adsorbent Fe–Mg-type hydrotalcite and its adsorption capability of As(III) and Cr(VI) from aqueous solution, J. Ind. Eng. Chem., 59 (2018) 56–63.
[4] S.F. Li, Y. Guo, M. Xiao, T. Zhang, S.H. Yao, S.Y. Zang, H.T. Fan, Y.M. Shen, Z.G. Zhang, W.X. Li, Enhanced arsenate removal from aqueous solution by Mn-doped MgAl-layered double hydroxides, Environ. Sci. Pollut. Res., 26 (2019) 12014–12024.
[5] Y.F. Jia, G.P. Demopoulos, Coprecipitation of arsenate with iron(III) in aqueous sulfate media: effect of time, lime as base and co-ions on arsenic retention, Water Res., 42 (2008) 661–668.
[6] E.K. Mroczek, D. Graham, L. Bacon, Removal of arsenic and silica from geothermal fluid by electrocoagulation, J. Environ. Chem. Eng., 7 (2019) 103232.
[7] M. Kobya, M.S. Öncel, E. Demirbas, M. Celen, Arsenic and boron removal from spring and groundwater samples in boron mining regions of Turkey by electrocoagulation and ion-exchange consecutive processes, Desal. Water Treat., 93 (2017) 288–296.

[8] C.-G. Lee, P.J.J. Alvarez, A. Nam, S.-J. Park, T.G. Do, U.-S. Choi, S.-H. Lee, Arsenic(V) removal using an amine-doped acrylic ion exchange fiber: Kinetic, equilibrium, and regeneration studies, J. Hazard. Mater., 325 (2017) 223–229.
[9] H.-T. Fan, X.L. Fan, J. Li, M.M. Guo, D.S. Zhang, F. Yan, T. Sun, Selective removal of arsenic(V) from aqueous solution using a surface-ion-imprinted amine-functionalized silica gel sorbent, Ind. Eng. Chem. Res., 51 (2012) 5216–5223.
[10] X.W. Liu, M.L. Gao, W.W. Qiu, Z.H. Khan, N.B. Liu, L. Lin, Z.G. Song, Fe–Mn–Ce oxide-modified biochar composites as efficient adsorbents for removing As(III) from water: adsorption performance and mechanisms, Environ. Sci. Pollut. Res., 26 (2019) 17373–17382.
[11] L.L. Hao, N. Wang, C. Wang, G. Li, Arsenic removal from water and river water by the combined adsorption – UF membrane process, Chemosphere, 202 (2018) 768–776.
[12] A. Criscuoli, P. Bafaro, E. Drioli, Vacuum membrane distillation for purifying waters containing arsenic, Desalination, 323 (2013) 17–21.
[13] H.J. Zhu, Y.F. Jia, X. Wu, H. Wang, Removal of arsenic from water by supported nano zero-valent iron on activated carbon, J. Hazard. Mater., 172 (2009) 1591–1596.
[14] S.H. Yao, Y.F. Jia, S.L. Zhao, Photocatalytic oxidation and removal of arsenite by titanium dioxide supported on granular activated carbon, Environ. Technol., 33 (2012) 983–988.
[15] X. Ge, Y. Ma, X.Y. Song, G.Z. Wang, H.M. Zhang, Y.X. Zhang, H.J. Zhao, β-FeOOH nanorods/carbon foam-based hierarchically porous monolith for highly effective arsenic removal, ACS Appl. Mater. Interfaces, 9 (2017) 13480−13490.
[16] A. Habineza, J. Zhai, T. Ntakirutimana, F.P. Qiu, X.T. Li, Q.F. Wang, Heavy metal removal from wastewaters by agricultural waste low-cost adsorbents: hindrances of adsorption technology to the large scale industrial application – a review, Desal. Water Treat., 78 (2017) 192−214.
[17] T.G. Asere, C.V. Stevens, G.D. Laing, Use of (modified) natural adsorbents for arsenic remediation: a review, Sci. Total Environ., 676 (2019) 706–720.
[18] H.-T. Fan, Y. Sun, Q. Tang, W.-L. Li, T. Sun, Selective adsorption of antimony(III) from aqueous solution by ion-imprinted organic–inorganic hybrid sorbent: kinetics, isotherms and thermodynamics, J. Taiwan Inst. Chem. Eng., 45 (2014) 2640–2648.
[19] H.-T. Fan, W. Sun, B. Jiang, Q.-J. Wang, D.-W. Li, C.-C. Huang, K.-J. Wang, Z.-G. Zhang, W.-X. Li, Adsorption of antimony(III) from aqueous solution by mercapto-functionalized silica-supported organic–inorganic hybrid sorbent: mechanism insights, Chem. Eng. J., 286 (2016) 128–138.
[20] D.X. Guo, Y.P. Zhao, H.D. Yang, S.F. Li, X. Fan, X.Y. Wei, Synthesis of Mg/Al layered double hydroxides from a sub-bituminous coal ash and their application in hexavalent chromium removal from aqueous solution, Desal. Water Treat., 139 (2019) 191–201.
[21] H.-T. Fan, Q. Tang, Y. Sun, Z.-G. Zhang, W.-X. Li, Selective removal of antimony(III) from aqueous solution using antimony(III)-imprinted organic–inorganic hybrid sorbents by combination of surface imprinting technique with sol–gel process, Chem. Eng. J., 258 (2014) 146–156.
[22] T. Tatarchuk, N. Paliychuk, R.B. Bitra, A. Shyichuk, Mu. Naushad, I. Mironyuk, D. Ziółkowska, Adsorptive removal of toxic Methylene Blue and Acid Orange 7 dyes from aqueous medium using cobalt-zinc ferrite nanoadsorbents, Desal. Water Treat., 150 (2019) 374–385.
[23] T. Tatarchuk, A. Shyichuk, I. Mironyuk, Mu. Naushad, A review on removal of uranium(VI) ions using titanium dioxide based sorbents, J. Mol. Liq., 293 (2019) 11563.
[24] I. Mironyuk, T. Tatarchuk, H. Vasylyeva, V.M. Gun'ko, I. Mykytyn, Effects of chemosorbed arsenate groups on the mesoporous titania morphology and enhanced adsorption properties towards Sr(II) cations, J. Mol. Liq., 282 (2019) 587–597.
[25] I. Mironyuk, T. Tatarchuk, Mu. Naushad, H. Vasylyeva, I. Mykytyn, Highly efficient adsorption of strontium ions by carbonated mesoporous TiO_2, J. Mol. Liq., 285 (2019) 742–753.
[26] A.I.A. Sherlala, A.A.A. Raman, M.M. Bello, A. Buthiyappan, Adsorption of arsenic using chitosan magnetic graphene oxide nanocomposite, J. Environ. Manage., 246 (2019) 547–556.
[27] L.E. Verduzco, J. Oliva, A.I. Oliva, E. Macias, C.R. Garcia, M. Herrera-Trejo, N. Pariona, A.I. Mtz-Enriquez, Enhanced removal of arsenic and chromium contaminants from drinking water by electrodeposition technique using graphene composites, Mater. Chem. Phys., 229 (2019) 197–209.
[28] C. Wang, J. Luan, C. Wu, Metal-organic frameworks for aquatic arsenic removal, Water Res., 158 (2019) 370–382.
[29] S.I. Siddiqui, S.A. Chaudhry, A review on graphene oxide and its composites preparation and their use for the removal of As^{3+} and As^{5+} from water under the effect of various parameters: application of isotherm, kinetic and thermodynamics, Process Saf. Environ. Prot., 119 (2018) 138−163.
[30] D.E. Giles, M. Mohapatra, T.B. Issa, S. Anand, P. Singh, Iron and aluminium based adsorption strategies for removing arsenic from water, J. Environ. Manage., 92 (2011) 3011−3022.
[31] S.I. Siddiqui, S.A. Chaudhry, Iron oxide and its modified forms as an adsorbent for arsenic removal: a comprehensive recent advancement, Process Saf. Environ. Prot., 111 (2017) 592–626.
[32] Z.X. Zhao, Y.F. Jia, L.Y. Xu, S.L. Zhao, Adsorption and heterogeneous oxidation of As(III) on ferrihydrite, Water Res., 45 (2011) 6496−6504.
[33] X.J. Guo, Z.J. Wu, M.C. He, X.G. Meng, X. Jin, N. Qiu, J. Zhang, Adsorption of antimony onto iron oxyhydroxides: adsorption behavior and surface structure, J. Hazard. Mater., 276 (2014) 339−345.
[34] R. Ozola, A. Krauklis, M. Leitietis, J. Burlakovs, I. Vircava, L. Ansone-Bertina, A. Bhatnagar, M. Klavins, FeOOH-modified clay sorbents for arsenic removal from aqueous solutions, Environ. Technol. Innovation, 13 (2019) 364–372.
[35] F.H. Li, D. Geng, Q. Cao, Adsorption of As(V) on aluminum-, iron-, and manganese-(oxyhydr)oxides: equilibrium and kinetics, Desal. Water Treat., 56 (2015) 1829−1838.
[36] Y. Mamindy-Pajany, C. Hurel, N. Marmier, M. Roméo, Arsenic adsorption onto hematite and goethite, C.R. Chim., 12 (2009) 876−881.
[37] H. Li, W. Li, Y.J. Zhang, T.S. Wang, B. Wang, W. Xu, L. Jiang, W.G. Song, C.Y. Shu, C.R. Wang, Chrysanthemum-like α-FeOOH microspheres produced by a simple green method and their outstanding ability in heavy metal ion removal, J. Mater. Chem., 21 (2011) 7878−7881.
[38] B. Wang, H.B. Wu, L. Yu, R. Xu, T.-T. Lim, X.W. Lou, Template-free formation of uniform urchin-like α-FeOOH hollow spheres with superior capability for water treatment, Adv. Mater., 24 (2012) 1111–1116.
[39] Y.M. Dong, H.X. Yang, R.C. Rao, A.M. Zhang, Selective synthesis of α-FeOOH and α-Fe_2O_3 nanorods via a temperature controlled process, J. Nanosci. Nanotechnol., 9 (2009) 4774–4779.
[40] M. Xiao, Y.P. Zhao, S.F. Li, Facile synthesis of chrysanthemum-like mesoporous α-FeOOH and its adsorptive behavior of antimony from aqueous solution, J. Dispersion Sci. Technol., (2019) doi: 10.1080/01932691.2019.1637263.
[41] U. Schwertmann, R.M. Cornell, Iron Oxides in the Laboratory: Preparation and Characterization, VCH, Weinheim and New York, 2000.
[42] S.F. Li, F. Qi, M. Xiao, H. Fan, Y.M. Shen, K. Du, Z.G. Zhang, W.X. Li, *In situ* synthesis of layered double hydroxides on γ-Al_2O_3 and its application in chromium(VI) removal, Water Sci. Technol., 75 (2017) 1466−1473.
[43] S.F. Li, T.T. You, Y. Guo, S.H. Yao, S.Y. Zang, M. Xiao, Z.G. Zhang, Y.M. Shen, High dispersions of nano zero valent iron supported on biochar by one-step carbothermal synthesis and its application in chromate removal, RSC Adv., 9 (2019) 12428−12435.
[44] E. Bazrafshan, M. Sobhanikia, F.K. Mostafapour, H. Kamani, D. Balarak, Chromium biosorption from aqueous environments by mucilaginous seeds of *Cydonia oblonga*: thermodynamic, equilibrium and kinetic studies, Global Nest J., 19 (2017) 269–277.
[45] S. Agarwal, I. Tyagi, V.J. Gupta, M.H. Dehghani, J. Jaafari, D. Balarak, M. Asif, Rapid removal of noxious nickel(II) using novel γ-alumina nanoparticles and multiwalled carbon

nanotubes: kinetic and isotherm studies, J. Mol. Liq., 224 (2016) 618–623.
[46] M. Stachowicz, T. Hiemstra, W.H. van Riemsdijk, Multi-competitive interaction of As(III) and As(V) oxyanions with Ca^{2+}, Mg^{2+}, PO_4^{3-}, and CO_3^{2-} ions on goethite, J. Colloid Interface Sci., 320 (2008) 400–411.
[47] D. Balarak, H. Azarpira, F.K. Mostafapour, Thermodynamics of removal of cadmium by adsorption on Barley husk biomass, Der Pharma Chem., 8 (2016) 243–247.
[48] H. Azarpira, Y. Mahdavi, Removal of Cd(II) by adsorption on agricultural waste biomass, Der Pharma Chem., 8 (2016) 61–67.
[49] D. Balarak, A. Joghataei, H. Azarpira, F.K. Mostafapour, Isotherms and thermodynamics of Cd(II) ion removal by adsorption onto azolla filiculoides, Int. J. Pharm. Technol., 8 (2016) 15780–15788.
[50] Y.F. Jia, L.Y. Xu, X. Wang, G.P. Demopoulos, Infrared spectroscopic and X-ray diffraction characterization of the nature of adsorbed arsenate on ferrihydrite, Geochim. Cosmochim. Acta, 71 (2007) 1643–1654.
[51] J.J. Du, J.L. Cui, C.Y. Jing, Rapid in situ identification of arsenic species using a portable Fe_3O_4@Ag SERS sensor, Chem. Commun., 50 (2014) 347–349.
[52] B. Hudcová, V. Veselská, J. Filip, S. Číhalová, M. Komárek, Sorption mechanisms of arsenate on Mg-Fe layered double hydroxides: a combination of adsorption modeling and solid state analysis, Chemosphere, 168 (2017) 539–548.
[53] S. Hasan, A. Ghosh, K. Race, R. Schreiber Jr., M. Prelas, Dispersion of FeOOH on chitosan matrix for simultaneous removal of As(III) and As(V) from drinking water, Sep. Sci. Technol., 49 (2014) 2863–2877.
[54] Y. Jia, X.-Y. Yu, T. Luo, M.-Y. Zhang, J.-H. Liu, X.-J. Huang, Two-step self-assembly of iron oxide into three-dimensional hollow magnetic porous microspheres and their toxic ion adsorption mechanism, Dalton Trans., 42 (2013) 1921–1928.
[55] D. Budimirović, Z.S. Veličković, V.R. Djokić, M. Milosavljević, J. Markovski, S. Lević, A.D. Marinković, Efficient As(V) removal by α-FeOOH and α-FeOOH/α-MnO_2 embedded PEG-6-arm functionalized multiwall carbon nanotubes, Chem. Eng. Res. Des., 119 (2017) 75–86.
[56] Y. Jia, T. Luo, X.Y. Yu, B. Sun, J.-H. Liu, X.-J. Huang, Synthesis of monodispersed α-FeOOH nanorods with a high content of surface hydroxyl groups and enhanced ion-exchange properties towards As(V), RSC Adv., 3 (2013) 15805–15811.
[57] M.P. Asta, J. Cama, M. Martínez, J. Giménez, Arsenic removal by goethite and jarosite in acidic conditions and its environmental implications, J. Hazard. Mater., 171 (2009) 965–972.
[58] A.T. Jacobson, M.H. Fan, Evaluation of natural goethite on the removal of arsenate and selenite from water, J. Environ. Sci., 76 (2019) 133–141.
[59] A.C.Q. Ladeira, V.S. Ciminelli, Adsorption and desorption of arsenic on an oxisol and its constituents, Water Res., 38 (2004) 2087–2094.

Supplementary information

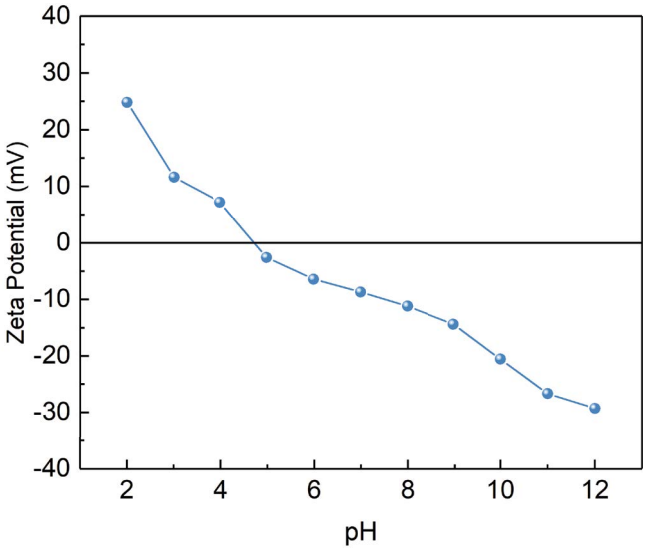

Fig. S1. Zeta potential profile of mesoporous goethite vs. pH in aqueous solution.

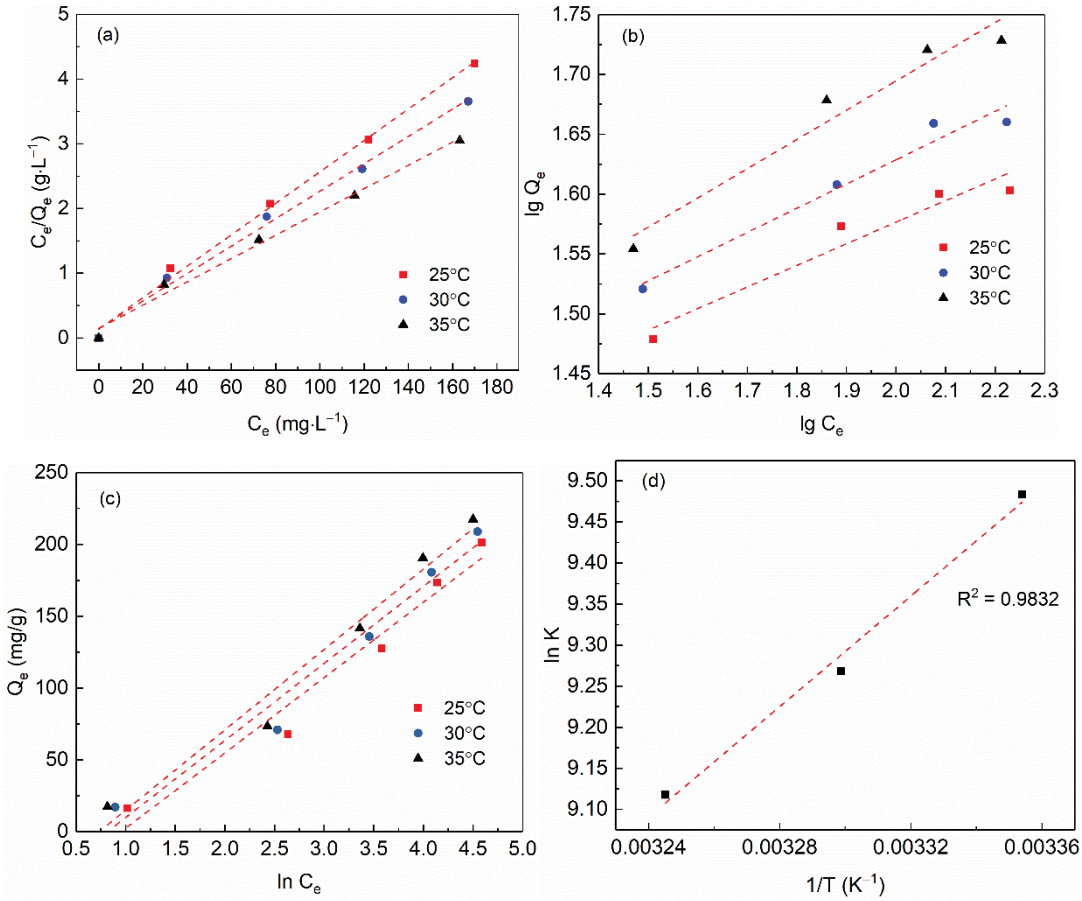

Fig. S2. (a) Langmuir model fitting, (b) Freundlich model fitting, (c) Temkin model fitting for As(V) adsorption isotherms on mesoporous goethite, and (d) the plot of ln$k$ vs. 1/T with Langmuir model.